

LONG-TERM SPECTRAL VARIATIONS OF ULTRALUMINOUS X-RAY SOURCES IN THE INTERACTING GALAXY SYSTEMS M 51 AND NGC 4490/85

TESSEI YOSHIDA^{1,2}, KEN EBISAWA¹, KYOKO MATSUSHITA², MASAHIRO TSUJIMOTO¹, AND TOSHIHIRO KAWAGUCHI³

Draft version August 26, 2010

ABSTRACT

Variable ultraluminous X-ray sources (ULXs), which are considered to be black hole binaries (BHBs), are known to show state transitions similarly to Galactic BHBs. However, the relation between the ULX states and the Galactic BHB states is still unclear primarily due to less well-understood behaviors of ULXs in contrast to the Galactic BHBs. Here, we report a statistical X-ray spectral study of 34 energy spectra from seven bright ULXs in the interacting galaxy systems M 51 and NGC 4490/85, using archive data from multiple *Chandra* and *XMM-Newton* observations spanning for a few years. In order to compare with Galactic BHB states, we applied representative spectral models of BHBs; a power-law (PL), a multi-color disk black body (MCD), and a slim disk model to all the ULX spectra. We found a hint of a bimodal structure in the luminosity distribution of the samples, suggesting that ULXs have two states with typical luminosities of $3\text{--}6 \times 10^{39}$ and $1.5\text{--}3 \times 10^{39}$ ergs s⁻¹. Most spectra in the brighter state are explained by the MCD or the slim disk model, whereas those in the fainter state are explained by the PL model. In particular, the slim disk model successfully explains the observed spectral variations of NGC 4490/85 ULX-6 and ULX-8 by changes of the mass accretion rate to a black hole of an estimated mass of $< 40 M_{\odot}$. From the best-fit model parameters of each state, we speculate that the brighter state in these two ULXs corresponds to the brightest state of Galactic BHBs, which is often called the “apparently standard state”. The fainter state of the ULXs has a PL shaped spectrum, but the photon index range is much wider than that seen in any single state of Galactic BHBs. We thus speculate that it is a state unique to ULXs. Some sources show much fainter and steeper spectra than the faint state, which we identified as another state.

Subject headings: accretion, accretion disks — black hole physics — galaxies: individual (M 51, NGC 4490, NGC 4485) — X-rays: binaries

1. INTRODUCTION

Ultraluminous X-ray sources (ULXs) are off-nuclear point-like sources detected in the X-ray bandpass with luminosities of $\geq 10^{39\text{--}41}$ ergs s⁻¹; see Liu, & Bregman (2005), Fabbiano (2006) for a review. Most variable ULXs are considered to be black hole binaries (BHBs) based on observational characteristics similar to Galactic BHBs, such as short- and long-term variations (e.g. Ptak, & Griffiths 1999), thermal disk emission (e.g. Makishima et al. 2000; Feng & Kaaret 2010), and state transitions (e.g. Kubota et al. 2001). The large luminosity of ULXs suggests the black hole (BH) mass (M) to be much larger than that of Galactic BHs ($\sim 10 M_{\odot}$) under the assumption that the radiation is spherically symmetric and the observed luminosity does not exceed the Eddington luminosity $L_{\text{Edd}} = 1.5 \times 10^{38} (M/M_{\odot})$ ergs s⁻¹.

Three competing interpretations have been proposed for ULXs. The first is that ULXs contain a so-called intermediate mass BH with a mass of 100–1000 M_{\odot} (Miller, & Colbert 2004). In fact, a large mass of $\gtrsim 700 M_{\odot}$ is suggested for M 82 X-1 based on its large luminosity (Matsumoto et al. 2001; Kaaret et al. 2001). The second is that ULXs are BHs with a mass compa-

rable to or slightly larger than that of Galactic BHs of $< 40 M_{\odot}$ (so-called stellar mass BHs; Ebisawa et al. 2003; Okajima et al. 2006). The super-Eddington luminosity is interpreted as a consequence of the ULXs having a slim disk (Abramowicz et al. 1988) rather than the standard disk (Shakura, & Sunyaev 1973). In the state expressed by the slim disk model, which is a stable solution for very high mass accretion rates of $\gtrsim 8 \times 10^{18} (M/M_{\odot})$ g s⁻¹, the emission is moderately collimated toward the direction normal to the disk so that the luminosity can be super-Eddington (e.g. Ohsuga et al. 2005). The third is the beaming model with a high collimation (King et al. 2001), although the scenario may have difficulties in explaining extended photoionized nebulae found around some ULXs. For example, Kaaret et al. (2004) studied the Holmberg II ULX within an extended nebula. The nebula emits He II 4686 Å line relatively isotropically, which is produced by the X-ray photoionization from the central ULX. Thus, the extended nebula is unlikely excited by highly collimated radiation.

Galactic BHBs are known to show transitions among several states (Esin et al. 1997). The most three well-established states are the low-hard state (LHS), the high-soft state (HSS), and the very high state (VHS). In general, the LHS is the faintest state ($0.01\text{--}0.04 L_{\text{Edd}}$, Maccarone 2003), which shows a power-law (PL) spectrum with a photon index $\Gamma = 1.5\text{--}1.9$ (Esin et al. 1997). The HSS is generally brighter than the LHS, and is a thermal state with a convex-shaped spectrum. The spectrum can be fitted by a multi-color disk black body (MCD) model (Pringle 1981), which is an approximation

Electronic address: yoshida.tessei@ac.jaxa.jp

¹ Japan Aerospace Exploration Agency, Institute of Space and Astronautical Science, 3-1-1 Yoshinodai, Chuo, Sagami-hara, Kanagawa 252-5210, Japan

² Department of Physics, Tokyo University of Science, 1-3 Kagurazaka, Shinjuku, Tokyo 162-8601, Japan

³ Center for Computational Sciences, University of Tsukuba, 1-1-1 Tennodai, Tsukuba, Ibaraki 305-8577, Japan

for the standard disk spectra. The VHS usually shows an X-ray luminosity comparable or higher than that of the HSS and a steep PL-like spectrum (typically $\Gamma \sim 2.5$, Esin et al. 1997). The spectrum is considered to be a mixture of a weak disk component and a strong Comptonized component.

In addition to these well-established three states, yet another state — the apparently standard state (ASS) — was proposed by Kubota, & Makishima (2004). The ASS is a thermal state, which is brighter ($L_X \gtrsim 0.3 L_{\text{Edd}}$) than the other states. At least two Galactic BHBs are reported to show this state: XTE J1550–564 (Kubota, & Makishima 2004) and 4U 1630–47 (Abe et al. 2005). The spectral shape in the ASS is better represented by a slim disk model than the MCD model. If the spectra in this state are fitted with the MCD model, the following three anomalies appear (Kubota, & Makishima 2004; Abe et al. 2005): (i) Excess emission is found below 5 keV and above 10 keV. (ii) The innermost disk temperature is higher than that in the HSS. (iii) The innermost disk radius tends to decrease with the increasing the disk temperature. In the HSS, in contrast, the innermost disk temperature is rather constant (e.g. Ebisawa et al. 1994). Some of these anomalies can be solved either by using the slim-disk model instead of the MCD model (Kubota, & Makishima 2004; Abe et al. 2005), or by introducing spectral hardening to the MCD model as a function of accretion rate (Davis et al. 2006; McClintock et al. 2007). Although it is yet unclear if the ASS should be considered to be an independent state or an extension of the HSS, we treat the four states (LHS, HSS, VHS, and ASS) as different states in this paper.

Similarly to the Galactic BHBs, some ULXs are known to show state transitions in timescales of months to years between two different spectral states. In the case of IC 342 sources 1 and 2, Kubota et al. (2001) dubbed them the “hard” and the “soft” state, which respectively has a spectrum with a PL and a convex shape. The latter is brighter than the former by from a factor of a few to one order of magnitude. However, the relation between the spectral states of ULXs and those of Galactic BHBs is still unclear. Observational clues will be obtained by comparing the state transitions, including their frequencies and time scales of transitions.

ULXs are less well frequently monitored than Galactic BHBs, and their time variation is less understood. Obviously, increasing the samples of ULXs is a key to conduct statistical studies of state transitions. Nearby (<5 Mpc) galaxies and interacting galaxy systems at a moderate distance (5–10 Mpc) are two suitable laboratories for this purpose. ULXs in nearby galaxies are bright in flux and can be examined in detail. About 15 ULXs were studied within 5 Mpc, which includes NGC 1313 X-1 and 2 (Mizuno et al. 2007), IC 342 sources 1 and 2 (Kubota et al. 2001), Holmberg II X-1 (Goad et al. 2006), M 81 X-9 (Tsunoda et al. 2006), M 82 X-1 (Miyawaki et al. 2009), and NGC 5204 X-1 (Roberts et al. 2006).

We focus on the other laboratory; ULXs in interacting galaxy systems. They are more distant and fainter in flux than those in nearby galaxies. However, the average number of ULX per galaxy is much larger, enabling us to monitor a large number of samples at the same distance

TABLE 1
OBSERVATION LOG.

Data label	Observatory	ObsID	Date	t_{exp}^a (ks)
M 51				
C1	<i>Chandra</i>	354	2000-06-20	14.9
C2		1622	2001-06-23	26.8
C3		3932	2003-08-07	48.0
X1	<i>XMM-Newton</i>	0112840201	2003-01-15	20.7/19.0
X2		0212480801	2005-07-01	49.0/47.3
X3		0303420101	2006-05-20	52.5/52.2
X4		0303420201	2006-05-24	36.6/34.9
NGC 4490/85				
C1'	<i>Chandra</i>	1579	2000-11-03	19.5
C2'		4725	2004-07-29	38.5
C3'		4726	2004-11-20	39.6
X1'	<i>XMM-Newton</i>	0112280201	2002-05-27	17.4/11.9

^a ACIS exposure for the *Chandra* observations and EPIC MOS (left) and EPIC pn (right) exposure for the *XMM-Newton* observations.

simultaneously. The number of ULXs in nine interacting systems at 20–100 Mpc (Brassington et al. 2007) averages to be >6 ULXs system⁻¹.

Within 10 Mpc, the M 51 system and the NGC 4490 and NGC 4485 system (hereafter called NGC 4490/85) host the largest number of ULXs. The former at ~ 8.4 Mpc (Feldmeier et al. 1997) hosts nine, while the latter at ~ 8 Mpc (de Vaucouleurs et al. 1976) hosts eight. Both systems have been observed several times in X-rays and thus are suitable to study long-term variations of multiple ULXs at a time. The X-ray data from these two systems have not been uniformly analyzed yet. In this paper, we apply physical models to the spectra of these ULXs and give interpretations to the observed long-term spectral changes, in comparison with the Galactic BHB state transitions.

2. OBJECTS

2.1. M 51

M 51 is one of the closest interacting galaxy systems, which is composed of two spiral galaxies, NGC 5194 and NGC 5195. The sizes of NGC 5194 and NGC 5195 are 27 and 14 kpc from the isophotal diameters $11''.2$ and $5''.8$ (de Vaucouleurs et al. 1991), respectively. The total mass of the M 51 system is $\sim 1.5 \times 10^{11} M_{\odot}$ (Kuno, & Nakai 1997), and the mass of NGC 5194 is larger than that of NGC 5195 by a factor of a few (Schweizer 1977).

Radio observations identified many H II regions (van der Hucht et al. 1988), indicating that the system has an on-going star forming activity at a star formation rate of $\sim 4 M_{\odot} \text{ yr}^{-1}$ (Scoville et al. 2001). Two (and possibly another) core-collapse supernovae (SNe) recently occurred in the galaxy⁴.

M 51 has been observed many times in X-rays by the *Einstein* (Palumbo et al. 1985), *ROSAT* (Marston et al. 1995; Ehle et al. 1995), *ASCA* (Terashima et al. 1998; Ptak et al. 1999), *BeppoSAX* (Fukazawa et al. 2001), *XMM-Newton* (Dewangan et al. 2005), and *Chandra* (Liu et al. 2002; Terashima, & Wilson 2004) observatories. The number of X-ray sources increased from three by *Einstein* (Palumbo et al. 1985) to 113 by *Chandra*

⁴ See <http://web.oapd.inaf.it/supern/cat/> for detail.

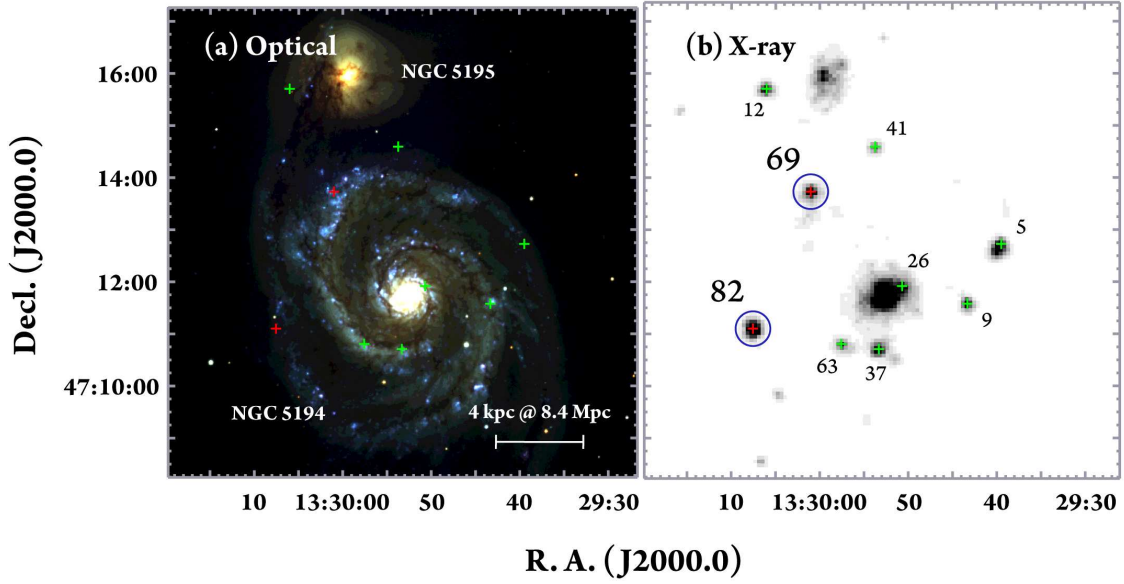


FIG. 1.— Optical and X-ray images of M51. (a) SDSS three color image. Red, green, and blue respectively represents the r -, g -, and u -band intensity. Pluses show positions of the nine ULXs in Dewangan et al. (2005); the two brightest sources, focused in this study, are shown in red and the remainders are in green. (b) Smoothed *XMM-Newton* MOS-1 image in the 0.5–8.0 keV band. Solid blue circles indicate the source extraction region.

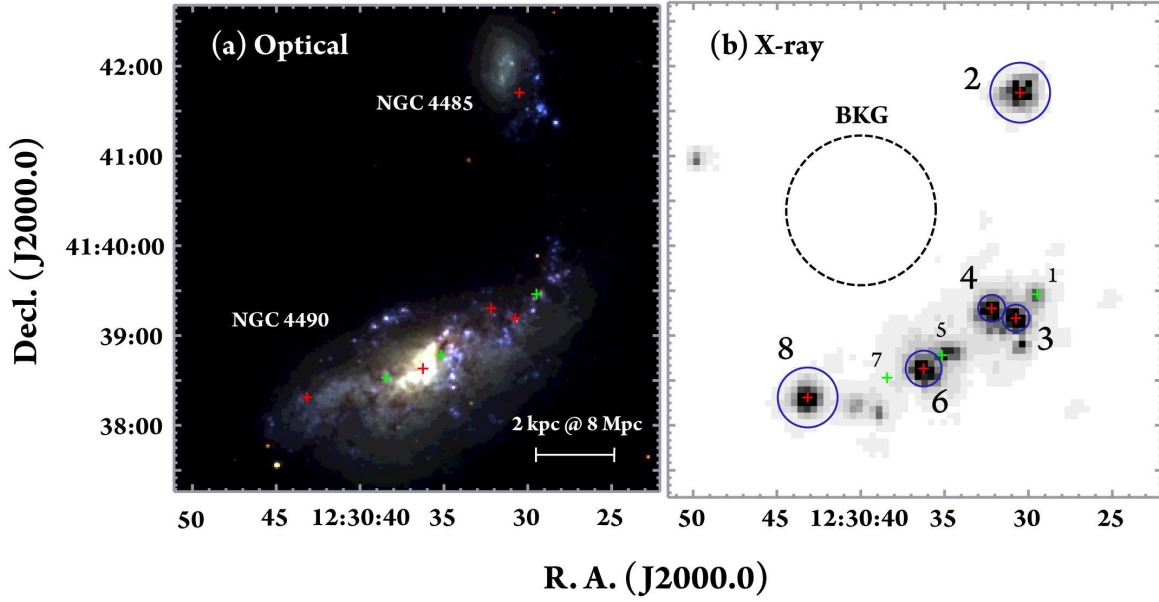


FIG. 2.— Same with Figure 1, but for NGC 4490/85. Pluses show positions of the eight ULXs in Fridriksson et al. (2008). The dashed circle in (b) indicates the common background region.

(Terashima, & Wilson 2004), which includes nine ULXs (Dewangan et al. 2005). We follow the nomenclature by Terashima, & Wilson (2004). Figure 1 (a) shows positions of the ULXs on the optical image by the Sloan Digital Sky Survey (SDSS) data. All ULXs are distributed along galactic arms. Terashima et al. (2006) reported using the *Hubble Space Telescope* data that four ULXs (sources-9, 37, 69, and 82) are located near the center or at the rim of star clusters. They also identified one or

more optical counterparts to six ULXs.

Previously published X-ray studies (e.g. Dewangan et al. 2005; Terashima et al. 2006) were based on four X-ray data sets among seven. We reduce all the available data including three unpublished sets.

2.2. NGC 4490/85

NGC 4490 and NGC 4485, the former being a spiral and the latter being an irregular galaxy,

are interacting with each other. NGC 4490/85 is one of the closest interacting galaxies as well as M51, belonging to the CVnII group of galaxies (de Vaucouleurs et al. 1976; Viallefond et al. 1980; Clemens et al. 1998, 1999; Fridriksson et al. 2008). The size and the mass of NGC 4490 are ~ 15 kpc (Clemens, & Alexander 2002) and $\sim 1.6 \times 10^{10} M_{\odot}$ (Viallefond et al. 1980), respectively, while those of NGC 4485 are ~ 5.6 kpc (Clemens, & Alexander 2002) and $\sim 2 \times 10^9 M_{\odot}$ (Clemens et al. 1999), respectively.

Radio observations identified many H II regions in NGC 4490, indicating an on-going star forming activity at a star formation rate of $\sim 4.7 M_{\odot} \text{ yr}^{-1}$ (Clemens et al. 1999; Clemens, & Alexander 2002). Two core-collapse SNe recently occurred in the galaxy⁴.

NGC 4490/85 was observed several times with the *ROSAT* (Read et al. 1997; Roberts, & Warwick 2000), *XMM-Newton*, and *Chandra* observatories (Roberts et al. 2002; Fridriksson et al. 2008). The number of known X-ray sources increased from five by *ROSAT* (Roberts, & Warwick 2000) to 38 by *Chandra* (Fridriksson et al. 2008), which include eight ULXs (ULX-1 to ULX-8). We follow the nomenclature by Fridriksson et al. (2008). Figure 2 (a) shows positions of the ULXs on the SDSS image. ULX-2 belongs to NGC 4485, while the others to NGC 4490. ULX-6 is close to but offset from the dynamical center of the galaxy (Roberts et al. 2002), and the other ULXs in NGC 4490 are distributed along galactic arms. Six of them were observed by the *Spitzer Space Telescope*. Five sources (ULX-2, 3, 4, 6, and 8) are likely to be an accreting X-ray source based on the detection of some characteristic features of highly ionized species in the mid-infrared spectra, while the remaining one (ULX-1) is more likely to be an SN remnant (Vázquez et al. 2007). Nevertheless, X-ray flux variation was found from ULX-1 (Fridriksson et al. 2008), leading to the speculation that this source is a ULX associated with the SN remnant.

Previous X-ray studies (Roberts et al. 2002; Fridriksson et al. 2008) presented long-term variations in flux and color in several ULXs and gave some phenomenological analysis. We present long-term spectral variations of all the bright ULXs along with more physical models.

3. OBSERVATIONS AND DATA REDUCTION

We selected data sets with an exposure time longer than 10 ks for detailed spectral analysis. Throughout this paper, we use X-ray events in the 0.5–8.0 keV energy band. For M51, we analyzed three *Chandra* and four *XMM-Newton* archived data sets (Table 1). We labeled the observations as C1-3 and X1-4, respectively. C1, C2, C3, and X1 were used by Liu et al. (2002), Terashima, & Wilson (2004), Dewangan et al. (2005), and Terashima et al. (2006).

For NGC 4490/85, we reduced all the archived data sets of *Chandra* and *XMM-Newton* (Table 1). The sets are the same with those used in Fridriksson et al. (2008) and Gladstone, & Roberts (2009). We labeled the *Chandra* and the *XMM-Newton* observations as C1'-3' and X1', respectively.

3.1. *Chandra*

The *Chandra X-ray Observatory* (Weisskopf et al. 2002) has an unprecedented spatial resolution of $\sim 0''.5$ at the optical axis. The *Chandra* observations were conducted using the Advanced CCD for Imaging and Spectroscopy (ACIS; Garmire et al. 2003), which covers an energy range of 0.5–8.0 keV. The data were taken with the full frame mode with the aim point in the S3 chip. The field of view (FOV) of the chip is $\sim 500'' \times 500''$, which contains the entire system of both M51 and NGC 4490/85.

Using the *Chandra* Interactive Analysis of Observations (CIAO) version 4.0 and the ACIS Extract package (Broos et al. 2002) version 2008-06-06, we extracted the source and background events and constructed the energy spectra. The source events were accumulated from a region around each source encircling 90% of photons of a point-like source. The background events were from an annulus around each source.

We list the number of counts for the ULXs identified in M51 (Dewangan et al. 2005) and NGC 4490/85 (Fridriksson et al. 2008) in Tables 2 and 3, respectively. Among all the ULXs, we focus on the sources with a total count of more than 1000 at least in one observation, which are practically bright enough for our spectral analysis. Seven sources are thus selected; sources-69 and 82 for M51, and ULX-2, 3, 4, 6, and 8 for NGC 4490/85.

3.2. *XMM-Newton*

The *XMM-Newton* (Jansen et al. 2001) observatory is equipped with the European Photon Imaging Camera (EPIC), which is comprised of three X-ray CCD cameras. Two of the cameras are MOS arrays (MOS-1 and MOS-2) having an on-axis spatial resolution of $\sim 5''$ and sensitivity in the 0.15–12 keV band (Turner et al. 2001), while the remaining one is a pn array having an on-axis resolution of $\sim 6''$ and sensitivity at 0.15–15 keV (Strüder et al. 2001). Both instruments have a FOV with a radius of 30–40', and cover the two studied systems entirely (Figures 1b and 2b). In the M51 observations, the thin (X1, X3, and X4) and medium (X2) filters were used. All cameras were operated with the full frame mode. In the NGC 4490/85 observation (X1'), the medium filter was used. The two MOS and pn cameras were operated with the full frame mode and the extended full frame mode, respectively.

We used the Science Analysis System (SAS) version 7.1.0 for extracting events and generating response files. Some high background time intervals were seen in all observations. For three observations (M51 X2, X3, and X4), we excluded intervals with count rates larger than the average by more than 3σ . For the remaining observations, we used all exposures because the effect is negligible with only a few counts in extracted source counts.

We focus on the seven sources selected in the *Chandra* data (Tables 2 and 3). The source extraction regions are shown in Figures 1 (b) and 2 (b). We chose the source region with a radius of 9–20'' to avoid contamination from other sources. In M51, the background regions were extracted from an annulus around each source to offset the global diffuse emission. In contrast, in NGC 4490/85, a common background region devoid of bright sources (Figure 2b) was adopted. The background events have ~ 100 counts for MOS and ~ 300 counts for pn.

TABLE 2
SOURCE AND BACKGROUND COUNTS FOR M 51.

Name ^a	Counts ^b								
	<i>Chandra</i>			<i>XMM-Newton</i>					
	C1	C2	C3	X1			X2		
				MOS-1	MOS-2	pn	MOS-1	MOS-2	pn
Source-5	213 (0.1)	163 (0.2)	397 (1.3)	321 (59)	352 (44)	917 (102)	392 (62)	441 (60)	850 (63)
Source-9	121 (0.1)	195 (0.2)	696 (1.2)	182 (71)	172 (79)	227 (143)	281 (75)	328 (102)	862 (246)
Source-26	92 (0.8)	229 (1.3)	375 (3.2)	349 (410)	456 (374)	1148 (1212)	520 (512)	535 (433)	1271 (1151)
Source-37	2 (0.2)	497 (0.3)	3 (0.5)	263 (97)	141 (87)	283 (244)	344 (139)	431 (148)	947 (326)
Source-41	196 (0.3)	352 (0.5)	554 (2.3)	137 (35)	129 (44)	384 (121)	254 (49)	245 (62)	576 (163)
Source-63	105 (0.2)	245 (0.3)	184 (0.6)	187 (81)	222 (78)	448 (217)	227 (123)	262 (138)	411 (234)
Source-69	463 (0.9)	42 (1.2)	1698 (3.6)	302 (97)	309 (107)	813 (329)	1137 (152)	1258 (200)	2679 (401)
Source-82	757 (0.3)	778 (0.5)	1791 (0.9)	513 (76)	514 (51)	465 (95)	561 (74)	603 (87)	... ^c
Source-12	191 (1.1)	332 (2.3)	466 (6.0)	195 (37)	178 (24)	462 (114)	176 (101)	121 (82)	321 (126)

<i>XMM-Newton</i>								
	X3			X4				
	MOS-1	MOS-2	pn	MOS-1	MOS-2	pn		
Source-5	509 (101)	466 (101)	411 (88)	536 (79)	514 (97)	451 (94)		
Source-9	117 (119)	130 (157)	... ^c	187 (81)	205 (89)	617 (236)		
Source-26	607 (668)	668 (596)	... ^c	420 (496)	474 (441)	376 (757)		
Source-37	277 (162)	265 (160)	... ^c	113 (113)	108 (124)	275 (252)		
Source-41	319 (95)	265 (82)	691 (167)	212 (43)	229 (57)	593 (110)		
Source-63	233 (141)	217 (138)	476 (193)	162 (88)	170 (101)	366 (207)		
Source-69	1114 (164)	1306 (237)	2887 (647)	1067 (173)	1209 (207)	2864 (561)		
Source-82	653 (87)	577 (107)	1448 (225)	461 (70)	458 (78)	1236 (194)		
Source-12	157 (67)	129 (66)	374 (118)	118 (50)	130 (38)	146 (91)		

^a The nomenclatures follow Dewangan et al. (2005). The two brightest ULXs, focused in this paper, are shown in the bold font.

^b Source counts (background counts). The background counts are normalized to the source extraction area.

^c The data are unavailable, because the source is located in a gap or a dead area of a chip.

TABLE 3
SOURCE AND BACKGROUND COUNTS FOR NGC 4490/85.

Name ^a	Counts ^b					
	<i>Chandra</i>			<i>XMM-Newton</i>		
	C1'	C2'	C3'	X1'		
				MOS-1	MOS-2	pn
ULX-1	239 (0.2)	424 (1.1)	305 (0.7)
ULX-2	1243 (0.8)	1772 (9.9)	1436 (0.9)	609 (23.5)	499 (21.0)	403 (50.2)
ULX-3	566 (0.3)	1148 (1.2)	1209 (1.0)	339 (4.8)	309 (4.2)	554 (10.2)
ULX-4	455 (0.4)	1291 (1.9)	1375 (1.3)	365 (4.8)	419 (4.2)	775 (10.2)
ULX-5	30 (0.8)	374 (1.7)	561 (1.5)
ULX-6	473 (0.8)	299 (1.9)	1347 (2.3)	444 (8.5)	481 (7.5)	897 (18.1)
ULX-7	0 (0.3)	1 (0.7)	749 (0.9)
ULX-8	780 (0.4)	1333 (1.2)	1762 (1.4)	525 (23.5)	484 (21.0)	811 (50.2)

^a The nomenclatures follow Fridriksson et al. (2008). The five brightest ULXs, focused in this paper, are shown in the bold font.

^b Same with Table 2.

4. DATA ANALYSIS AND RESULTS

Hereafter, we call each exposure of a source as a “sample”. The total number of the samples is 34, since there are two sources with seven exposures for M 51 and five sources with four exposures for NGC 4490/85.

4.1. Light Curves

Using the X-ray timing analysis package XRONOS version 5.2.1, we created the background-subtracted light curves of the seven ULXs. We binned the curves with 1000 s bin⁻¹ and fitted them with a constant flux model. For the *XMM-Newton* observations, we considered that the flux is variable when neither of the MOS and pn light curves are fitted with a constant model.

As a result, we found significant variations (95% significance) only from one source (M 51 source-69). This source showed a significant short-term variation in most samples (C1, C3, X2, X3, and X4). We confirmed the

periodicity of ~ 7000 s in the flux in C1 as was reported by Liu et al. (2002).

4.2. Spectra

Figure 3 shows the background-subtracted spectra of all the samples. All were binned with at least 20 counts bin⁻¹. All spectra are featureless. Some sources show flux variation among different observations.

4.2.1. Fitting Models

We used the X-ray spectral fitting package XSPEC version 11.3.2 for the spectral analysis. For the interstellar extinction, we used the **wabs** model (Morrison, & McCammon 1983); for the hydrogen column densities, we assumed the fixed Galactic extinction of 1.57×10^{20} cm⁻² for M 51 or 1.78×10^{20} cm⁻² for NGC 4490/85 (Dickey, & Lockman 1990) and a thawed additional extinction for each source. For the *XMM-*

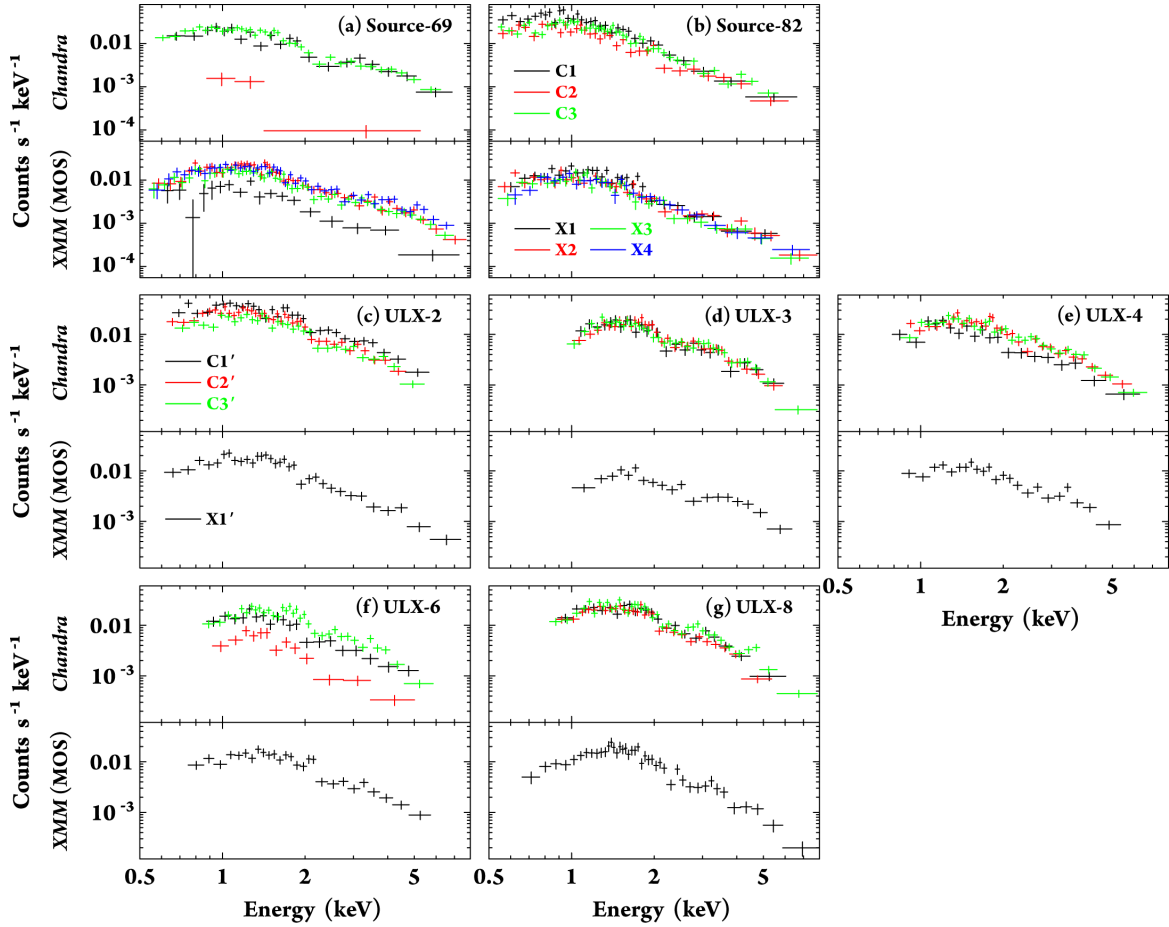


FIG. 3.— Time-averaged spectra of the seven ULXs. The top panels show the *Chandra* ACIS-S3 spectra by the three observations; C1, C1' (black), C2, C2' (red), and C3, C3' (green). The bottom panels show the *XMM-Newton* merged MOS spectra by the four (M51) or one (NGC 4490/85) observations; X1, X1' (black), X2 (red), X3 (green), and X4 (blue).

Newton EPIC data, we fitted the merged MOS and pn spectra simultaneously.

We first applied a PL model and an MCD model (diskbb in XSPEC; Mitsuda et al. 1984), which are commonly used to fit the continuum emission of Galactic BHBs and ULXs. The MCD model has the innermost disk temperature T_{in} as one of the parameters. Using the relation $L_{\text{bol}} = 4\pi(R_{\text{in}}/\xi)^2\sigma(T_{\text{in}}/\kappa)^4$, we can calculate the innermost disk radius R_{in} (Makishima et al. 2000). Here L_{bol} is the bolometric luminosity, σ is the Stefan-Boltzmann constant, $\kappa \sim 1.7$ is the spectral hardening factor (Shimura, & Takahara 1995), which is the ratio of the color temperature to the effective temperature, and $\xi = 0.412$ is the correction factor for the inner boundary condition (Kubota et al. 1998). For non-spinning BHs, the BH mass M_{BH} can be estimated from R_{in} using the relation $R_{\text{in}} = 8.86(M_{\text{BH}}/M_{\odot})$ km (Makishima et al. 2000). For the MCD model with $kT_{\text{in}} = 0.7\text{--}2.0$ keV, the 0.5–8.0 keV band contains $>80\%$ of the entire spectrum, thus we approximate the X-ray luminosity in this band as the bolometric luminosity.

We also fitted all the spectra with a slim disk model by Kawaguchi (2003)⁵. The “Kawaguchi model” takes into account of the Comptonization and the relativistic effects, and can constrain the BH mass and mass accretion rate as model parameters. We fixed the viscous

parameter α to be 0.1 (Vierdayanti et al. 2006). This model was successfully applied to some bright ULXs, including M33 X-8 (Foschini et al. 2006), NGC 1313 X-2, NGC 4559 X-7, X-10, NGC 5204 X-1 (Vierdayanti et al. 2006), and M82 X-1 (Okajima et al. 2006).

4.2.2. Fitting Results

We summarize all the best-fit parameters in Tables 4 and 5 for samples in M51 and NGC 4490/85, respectively. N_{H}' , Γ , and dM/dt indicate the absorption column density additional to that in our Galaxy, the photon index, and the mass accretion rate, respectively. Using the absorption-corrected flux ($f'_{\text{X,PL}}$, $f'_{\text{X,MCD}}$, and $f'_{\text{X,Kaw}}$ respectively for the PL, MCD, and Kawaguchi models), the luminosity is calculated as $L_{\text{X,PL}} = 4\pi D^2 f'_{\text{X,PL}}$, $L_{\text{X,MCD}} = 2\pi D^2 f'_{\text{X,MCD}}(\cos i)^{-1}$, and $L_{\text{X,Kaw}} = 2\pi D^2 f'_{\text{X,Kaw}}(\cos i)^{-1}$. Here, D is the distance to each galaxy, and i is the inclination of the disk. We assumed isotropic emission for the PL, and a moderate inclination for the MCD and Kawaguchi models ($i = 45^\circ$). Errors of all the parameters are calculated at the 90% confidence level. Figure 4 shows examples of the spectra and the best-fit models.

Although short-term flux and spectral hardness variation are found in M51 source-69 in C1, we averaged each exposure because the paucity of the counts do not allow us to conduct time-sliced spectroscopy. This source was very faint in C2, and N_{H}' is fixed at $6.0 \times 10^{20} \text{ cm}^{-2}$,

⁵ See <http://heasarc.nasa.gov/xanadu/xspec/models/slimdisk.html> for detail.

TABLE 4
BEST-FIT PARAMETERS FOR M 51.

Name	Data label	Model ^a	N'_{H} (10^{22} cm^{-2})	Γ	kT_{in} (keV)	R_{in} (km)	M_{BH} (M_{\odot})	dM/dt ($L_{\text{Edd}} \text{ c}^{-2}$)	L_{X} ($10^{38} \text{ ergs s}^{-1}$)	Red- χ^2 (d.o.f.)
Source-69	C1	P	< 0.08	$1.1^{+0.2}_{-0.1}$	27 ± 3	1.12(18)
		M	< 0.03	...	$2.3^{+1.2}_{-0.4}$	26^{+26}_{-9}	18^{+3}_{-2}	1.33(18)
		K	$0.15^{+0.07}_{-0.07}$	5^{+6}_{-3}	100^{+513}_{-71}	16^{+1}_{-3}	1.99(18)
	C2	P	0.06(fixed)	$3.1^{+1.1}_{-0.9}$	< 0.8	0.63(1)
		M	0.06(fixed)	...	$0.4^{+0.2}_{-0.1}$	123^{+143}_{-80}	< 0.4	0.14(1)
		K	0.06(fixed)	10^{+3}_{-6}	< 2	< 0.6	0.18(1)
	C3	P	$0.05^{+0.04}_{-0.04}$	$1.5^{+0.1}_{-0.1}$	29 ± 2	0.80(34)
		M	< 0.01	...	$1.5^{+0.2}_{-0.1}$	60^{+16}_{-10}	16 ± 1	1.94(34)
		K	$0.07^{+0.03}_{-0.03}$	7^{+4}_{-3}	100^{+335}_{-62}	19 ± 1	1.13(34)
	X1	P	$0.14^{+0.11}_{-0.06}$	$1.9^{+0.1}_{-0.2}$	12 ± 1	0.86(40)
		M	< 0.03	...	$1.2^{+0.2}_{-0.1}$	55^{+21}_{-13}	6.1 ± 0.6	1.19(40)
		K	$0.05^{+0.06}_{-0.05}$	< 9	> 425	7.5 ± 0.7	0.91(40)
	X2	P	$0.09^{+0.03}_{-0.03}$	$1.7^{+0.0}_{-0.1}$	52 ± 2	1.18(110)
		M	0.00	...	$1.5^{+0.1}_{-0.1}$	81^{+12}_{-9}	30 ± 1	2.03(110)
		K	$0.08^{+0.02}_{-0.02}$	12^{+2}_{-5}	100^{+254}_{-41}	34 ± 1	1.33(110)
	X3	P	$0.09^{+0.03}_{-0.03}$	$1.6^{+0.1}_{-0.1}$	41 ± 2	1.58(113)
		M	0.00	...	$1.7^{+0.1}_{-0.1}$	58^{+8}_{-9}	25 ± 1	2.23(113)
		K	$0.10^{+0.02}_{-0.02}$	10^{+1}_{-4}	100^{+154}_{-34}	27^{+2}_{-1}	1.76(113)
	X4	P	$0.10^{+0.03}_{-0.03}$	$1.5^{+0.1}_{-0.1}$	58 ± 2	1.41(111)
		M	< 0.01	...	$1.8^{+0.2}_{-0.1}$	60^{+10}_{-7}	35 ± 2	1.80(111)
		K	$0.13^{+0.02}_{-0.02}$	13^{+2}_{-5}	100^{+238}_{-30}	38^{+1}_{-2}	1.71(111)
Source-82	C1	P	$0.11^{+0.06}_{-0.06}$	$2.3^{+0.3}_{-0.2}$	28 ± 3	0.84(30)
		M	< 0.01	...	$0.7^{+0.1}_{-0.1}$	222^{+51}_{-47}	13 ± 1	1.48(30)
		K	$0.01^{+0.05}_{-0.01}$	34^{+7}_{-9}	7^{+3}_{-1}	15^{+2}_{-1}	0.95(30)
	C2	P	$0.02^{+0.03}_{-0.02}$	$1.9^{+0.2}_{-0.2}$	16 ± 1	1.13(30)
		M	< 0.01	...	$0.9^{+0.1}_{-0.1}$	121^{+38}_{-36}	8.5 ± 0.9	2.56(30)
		K	< 0.01	12^{+3}_{-5}	14^{+23}_{-5}	11 ± 1	1.31(30)
	C3	P	$0.12^{+0.05}_{-0.04}$	$2.1^{+0.1}_{-0.1}$	25 ± 2	1.60(34)
		M	< 0.01	...	$0.9^{+0.1}_{-0.1}$	146^{+21}_{-20}	12 ± 1	2.27(34)
		K	$0.04^{+0.03}_{-0.04}$	22^{+10}_{-8}	9^{+7}_{-2}	14 ± 1	1.72(34)
	X1	P	$0.21^{+0.07}_{-0.06}$	$2.6^{+0.3}_{-0.2}$	27^{+4}_{-3}	1.18(47)
		M	< 0.03	...	$0.7^{+0.1}_{-0.1}$	191^{+39}_{-40}	11 ± 1	1.91(47)
		K	$0.08^{+0.05}_{-0.05}$	37^{+9}_{-7}	5^{+1}_{-1}	13 ± 1	1.45(47)
	X2	P	< 0.04	$1.8^{+0.2}_{-0.1}$	19 ± 2	0.97(31)
		M	< 0.01	...	$1.0^{+0.2}_{-0.1}$	107^{+34}_{-29}	11 ± 1	2.58(31)
		K	< 0.01	11^{+2}_{-5}	20^{+58}_{-8}	13 ± 1	1.22(31)
	X3	P	$0.11^{+0.04}_{-0.04}$	$2.2^{+0.2}_{-0.1}$	17 ± 1	0.87(75)
		M	< 0.01	...	$0.8^{+0.1}_{-0.1}$	152^{+26}_{-25}	8.1 ± 0.5	1.80(75)
		K	$0.01^{+0.03}_{-0.01}$	17^{+5}_{-3}	7^{+4}_{-2}	9.6 ± 0.6	1.13(75)
	X4	P	$0.14^{+0.05}_{-0.04}$	$2.2^{+0.1}_{-0.2}$	20 ± 2	0.83(62)
		M	< 0.01	...	$0.9^{+0.1}_{-0.1}$	132^{+26}_{-25}	9.6 ± 0.6	1.47(62)
		K	$0.04^{+0.04}_{-0.04}$	19^{+8}_{-7}	8^{+7}_{-2}	11 ± 1	1.03(62)

^a The abbreviations for the models: “P” for PL, “M” for MCD (the *diskbb* model in XSPEC), and “K” for Kawaguchi model.

which is the median value obtained from the other six observations.

5. DISCUSSION

5.1. ULX Spectral States and Transitions

Based on the spectral fitting results presented in § 4, we investigate the spectral states of ULXs and their transitions. It is desirable that the states be defined for individual sources. However, given the low photon counts of each source, starting with individual details may lead to an unclear view. We thus first investigate the overall trend of all samples to constrain states of ULXs as a whole. In this section, we develop a discussion under the working hypothesis that all ULXs have a similar mass

and have the same states and follow a similar pattern of state transitions. The working hypothesis is checked with individual sources in § 5.2.

We constructed a histogram of the samples fitted successfully with the PL or the MCD model that represents PL-like and curved spectra, respectively (Figure 5). We consider that the fitting with a null hypothesis probability of $>5\%$ is successful. The best-fit luminosities derived by the PL fitting are used, because the derived luminosities hardly depend on the fitted models.

In the plot, it is noticeable that the fraction of successful fits by the MCD model is higher within the range of $3\text{--}6 \times 10^{39} \text{ ergs s}^{-1}$ for 20 samples and that by the PL model is higher within the range of $1.5\text{--}3 \times 10^{39} \text{ ergs s}^{-1}$

TABLE 5
BEST-FIT PARAMETERS FOR NGC 4490/85.

Name	Data label	Model ^a	N'_H (10^{22} cm^{-2})	Γ	kT_{in} (keV)	R_{in} (km)	M_{BH} (M_\odot)	dM/dt ($L_{\text{Edd}} c^{-2}$)	L_X ($10^{38} \text{ ergs s}^{-1}$)	Red- χ^2 (d.o.f.)
ULX-2	C1'	P	$0.21^{+0.08}_{-0.07}$	$1.6^{+0.2}_{-0.2}$	52 ± 4	1.69(28)
		M	$0.05^{+0.05}_{-0.05}$...	$1.6^{+0.2}_{-0.2}$	73^{+22}_{-17}	29 ± 2	1.34(28)
		K	$0.22^{+0.05}_{-0.04}$	12^{+12}_{-7}	100^{+506}_{-74}	35^{+3}_{-1}	1.68(28)
	C2'	P	$0.21^{+0.06}_{-0.06}$	$1.8^{+0.2}_{-0.2}$	40 ± 2	0.94(35)
		M	$0.05^{+0.04}_{-0.04}$...	$1.3^{+0.2}_{-0.1}$	92^{+22}_{-18}	20 ± 1	0.77(35)
		K	$0.18^{+0.04}_{-0.05}$	18^{+10}_{-13}	> 13	25^{+3}_{-2}	0.87(35)
	C3'	P	$0.28^{+0.08}_{-0.04}$	$1.8^{+0.1}_{-0.1}$	34 ± 2	1.63(28)
		M	$0.08^{+0.05}_{-0.05}$...	$1.4^{+0.2}_{-0.1}$	72^{+18}_{-15}	18 ± 1	1.28(28)
		K	$0.24^{+0.06}_{-0.07}$	15^{+7}_{-10}	> 14	22 ± 2	1.50(28)
	X1'	P	$0.27^{+0.07}_{-0.07}$	$2.1^{+0.1}_{-0.2}$	40^{+4}_{-3}	1.36(48)
		M	$0.02^{+0.05}_{-0.02}$...	$1.2^{+0.1}_{-0.1}$	97^{+21}_{-20}	19 ± 1	1.60(48)
		K	$0.16^{+0.04}_{-0.04}$	23^{+9}_{-6}	16^{+10}_{-4}	24 ± 2	1.40(48)
ULX-3	C1'	P	$0.82^{+0.35}_{-0.30}$	$2.0^{+0.4}_{-0.3}$	36^{+12}_{-7}	1.05(22)
		M	$0.37^{+0.24}_{-0.21}$...	$1.5^{+0.4}_{-0.3}$	65^{+38}_{-25}	18 ± 2	1.14(22)
		K	$0.65^{+0.21}_{-0.20}$	17^{+16}_{-13}	> 12	22 ± 4	1.06(22)
	C2'	P	$1.39^{+0.25}_{-0.23}$	$2.4^{+0.3}_{-0.3}$	58^{+21}_{-14}	0.63(30)
		M	$0.79^{+0.17}_{-0.15}$...	$1.2^{+0.2}_{-0.1}$	113^{+30}_{-25}	27 ± 2	0.67(30)
		K	$1.08^{+0.15}_{-0.15}$	40^{+8}_{-7}	14^{+5}_{-2}	33^{+5}_{-6}	0.60(30)
	C3'	P	$1.08^{+0.19}_{-0.17}$	$2.1^{+0.2}_{-0.2}$	51^{+9}_{-7}	0.90(33)
		M	$0.60^{+0.13}_{-0.12}$...	$1.4^{+0.2}_{-0.1}$	78^{+19}_{-16}	23 ± 2	0.84(33)
		K	$0.89^{+0.12}_{-0.11}$	29^{+6}_{-10}	17^{+11}_{-4}	29^{+5}_{-2}	0.82(33)
	X1'	P	$0.85^{+0.22}_{-0.20}$	$1.8^{+0.2}_{-0.1}$	44^{+8}_{-6}	1.00(33)
		M	$0.39^{+0.14}_{-0.13}$...	$1.8^{+0.3}_{-0.2}$	50^{+17}_{-13}	25 ± 2	1.10(33)
		K	$0.74^{+0.15}_{-0.10}$	12^{+15}_{-7}	> 23	29^{+4}_{-3}	1.00(33)
ULX-4	C1'	P	$0.49^{+0.20}_{-0.16}$	$1.9^{+0.3}_{-0.2}$	25^{+4}_{-3}	1.08(17)
		M	$0.22^{+0.13}_{-0.12}$...	$1.5^{+0.4}_{-0.3}$	55^{+29}_{-20}	13^{+3}_{-1}	1.15(17)
		K	$0.41^{+0.13}_{-0.12}$	12^{+6}_{-9}	> 12	16^{+2}_{-3}	1.08(17)
	C2'	P	$0.63^{+0.17}_{-0.15}$	$1.9^{+0.1}_{-0.2}$	51^{+7}_{-6}	1.36(29)
		M	$0.29^{+0.11}_{-0.10}$...	$1.5^{+0.2}_{-0.2}$	81^{+24}_{-19}	27 ± 2	1.24(29)
		K	$0.54^{+0.11}_{-0.11}$	26^{+9}_{-20}	> 16	33^{+5}_{-2}	1.29(29)
	C3'	P	$0.64^{+0.15}_{-0.06}$	$1.9^{+0.1}_{-0.1}$	42 ± 4	1.63(28)
		M	$0.34^{+0.09}_{-0.08}$...	$1.5^{+0.2}_{-0.2}$	70^{+17}_{-14}	22 ± 1	1.42(28)
		K	$0.57^{+0.09}_{-0.11}$	19^{+9}_{-14}	> 16	27 ± 2	1.53(28)
	X1'	P	$0.60^{+0.12}_{-0.11}$	$2.0^{+0.2}_{-0.1}$	50^{+7}_{-5}	1.32(44)
		M	$0.30^{+0.08}_{-0.07}$...	$1.3^{+0.1}_{-0.1}$	99^{+20}_{-17}	26 ± 2	0.98(44)
		K	$0.50^{+0.08}_{-0.07}$	34^{+5}_{-8}	17^{+7}_{-3}	31^{+3}_{-2}	1.14(44)
ULX-6	C1'	P	$0.35^{+0.23}_{-0.18}$	$1.8^{+0.2}_{-0.3}$	23^{+4}_{-3}	0.72(17)
		M	$0.10^{+0.15}_{-0.10}$...	$1.4^{+0.5}_{-0.3}$	53^{+37}_{-22}	12^{+2}_{-1}	0.79(17)
		K	$0.28^{+0.15}_{-0.12}$	10^{+7}_{-8}	> 11	15 ± 2	0.73(17)
	C2'	P	$0.60^{+0.35}_{-0.20}$	$2.6^{+0.6}_{-0.4}$	7^{+7}_{-3}	1.09(10)
		M	$0.15^{+0.22}_{-0.15}$...	$0.9^{+0.3}_{-0.2}$	64^{+41}_{-29}	$3.0^{+0.6}_{-0.5}$	1.45(10)
		K	$0.35^{+0.23}_{-0.21}$	12^{+7}_{-6}	15^{+4}_{-1}	$3.8^{+1.3}_{-1.0}$	1.24(10)
	C3'	P	$0.88^{+0.16}_{-0.14}$	$2.4^{+0.2}_{-0.2}$	53^{+10}_{-7}	1.49(31)
		M	$0.45^{+0.10}_{-0.09}$...	$1.1^{+0.1}_{-0.1}$	124^{+24}_{-21}	21^{+2}_{-1}	0.93(31)
		K	$0.65^{+0.10}_{-0.09}$	37^{+5}_{-4}	11^{+2}_{-2}	26 ± 2	1.06(31)
	X1'	P	$0.41^{+0.08}_{-0.08}$	$2.1^{+0.1}_{-0.1}$	44 ± 4	1.12(52)
		M	$0.11^{+0.05}_{-0.05}$...	$1.4^{+0.1}_{-0.1}$	86^{+16}_{-14}	23 ± 1	1.07(52)
		K	$0.30^{+0.05}_{-0.05}$	27^{+7}_{-7}	17^{+8}_{-4}	27^{+2}_{-3}	1.02(52)
ULX-8	C1'	P	$0.86^{+0.24}_{-0.20}$	$2.3^{+0.3}_{-0.3}$	56^{+15}_{-9}	1.45(20)
		M	$0.46^{+0.15}_{-0.13}$...	$1.2^{+0.2}_{-0.1}$	116^{+34}_{-28}	24 ± 2	0.96(20)
		K	$0.68^{+0.15}_{-0.14}$	37^{+8}_{-8}	12^{+5}_{-2}	30 ± 4	1.13(20)
	C2'	P	$0.90^{+0.16}_{-0.14}$	$2.6^{+0.2}_{-0.2}$	46^{+13}_{-9}	1.28(26)
		M	$0.43^{+0.10}_{-0.09}$...	$1.0^{+0.1}_{-0.1}$	147^{+28}_{-25}	19 ± 2	0.75(26)
		K	$0.60^{+0.12}_{-0.09}$	40^{+13}_{-5}	9^{+1}_{-2}	23^{+3}_{-2}	0.82(26)
	C3'	P	$0.74^{+0.12}_{-0.11}$	$2.0^{+0.2}_{-0.1}$	59^{+7}_{-5}	1.52(36)
		M	$0.38^{+0.08}_{-0.07}$...	$1.4^{+0.1}_{-0.1}$	90^{+18}_{-16}	28 ± 2	1.47(36)
		K	$0.61^{+0.08}_{-0.07}$	32^{+4}_{-10}	20^{+12}_{-4}	35 ± 4	1.41(36)
	X1'	P	$0.64^{+0.10}_{-0.09}$	$2.5^{+0.2}_{-0.2}$	54^{+9}_{-7}	0.88(58)
		M	$0.26^{+0.07}_{-0.06}$...	$1.0^{+0.1}_{-0.1}$	152^{+28}_{-25}	21 ± 1	0.92(58)
		K	$0.39^{+0.08}_{-0.06}$	38^{+10}_{-3}	10^{+1}_{-3}	26^{+2}_{-3}	0.86(58)

^a Same with Table 4.

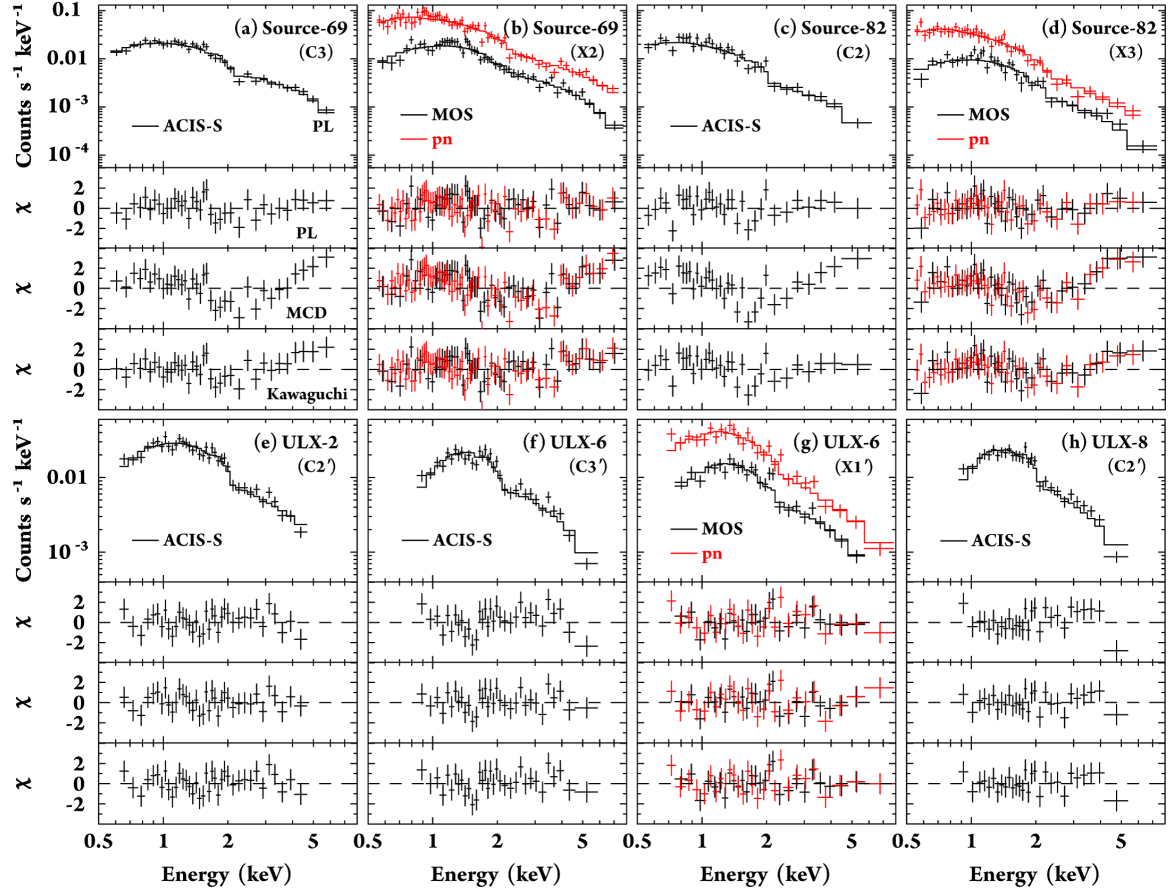


FIG. 4.— Examples of spectral fitting in M51 (a–d) and NGC 4490/85 (e–h). Spectra are shown for different sources with different instruments as indicated by the labels and colors. The top panels show the spectra (*pluses*) and the best-fit PL model (*solid histogram*), and the other panels show the residuals from the best-fit by a PL, MCD, and Kawaguchi model.

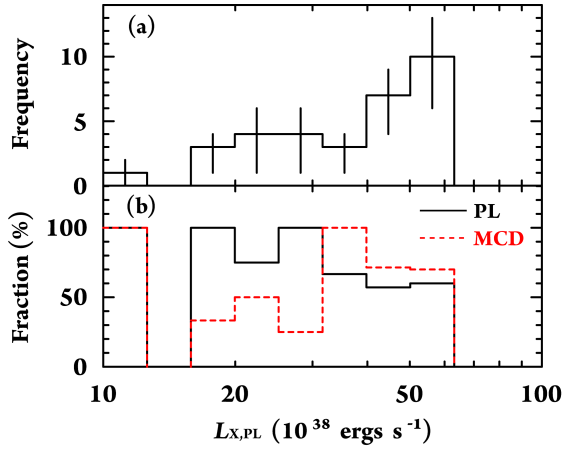


FIG. 5.— Luminosity distribution of (a) the number of samples and (b) the fraction of successful fits by the PL (black) and the MCD (red) models. The 1σ uncertainty, which is calculated from the Poisson distribution, is given in (a).

for 11 samples (Figure 5b). In order to test the claim statistically, we simulated numerous spectra containing the two components (PL and MCD) with randomly chosen parameters with varying contrasts, fitted them with one component model of either the PL or the MCD, and derived the fraction of the successful fits. As a result, we found no trend that the MCD model is favored toward brighter luminosity. Indeed, the PL model was favored. Thus, we consider that the higher fraction of successful MCD fits toward the brighter luminosity is not a statistical artifact.

The bimodal structure in the luminosity is unlikely to be explained by the bimodal distribution of the BH mass or the inclination of the system. This is because the distribution of the mass or the angle should be continuous, thus such a bimodal distribution is not natural. Rather, we speculate that there are two distinctive states corresponding to each luminosity range. We hereafter call them the “*bright*” state and the “*faint*” state. The two states match the “soft” and the “hard” states of the ULXs in Kubota et al. (2001). Based on the number of samples in each state, the frequency ratio *bright:faint* is about 2:1. The transition between the two occurs at $\sim 3 \times 10^{39}$ ergs s^{-1} (hereafter the “border luminosity”). Gladstone, & Roberts (2009) also claimed that the changes in spectral state occur at a similar luminosity of $\sim 2 \times 10^{39}$ ergs s^{-1} using samples in NGC 4490/85.

Some samples do not belong to either of the two states. Three samples (M51 source-69 in C2, X1, and NGC 4490/85 ULX-6 in C2') show luminosities fainter than the tail of the fainter range. These spectra may belong to the third state, which we call the “*dim*” state. We cannot constrain its representative spectral model for the paucity of statistics.

Two types of luminosity variation are recognized. We designate the variations within one state as the “*intra-state*” variations, and those across two or more states as the “*inter-state*” transitions.

5.2. Spectral Variations of Individual Sources

Now, we look into details of individual sources. The following result shows that the BH mass is in a range of $30\text{--}40 M_{\odot}$ for sources which we can estimate a mass with a representative model. This supports our assumption

to derive the overall trend in § 5.1. All the samples can be considered to be in one of the three states defined in § 5.1. The spectra in the *bright* state is explained better with a curved model and those in the *faint* state with a PL model. For the curved model, we see that the Kawaguchi model better explains the sources with sufficient constraints.

For each individual source, we discuss the states of all samples and the most likely representative model for each state. The result of spectral fitting is employed, which is mainly used to distinguish PL-like or curved spectra. If both the MCD and the Kawaguchi models give an acceptable fit for a curved spectrum, we further use a plot of $L_{X,MCD}$ against kT_{in} (Figure 6) to distinguish the two. The plot is commonly used for Galactic BHBs and ULXs. The two parameters are correlated in a different manner in two different physical conditions: standard disk or slim disk. If a system has a standard disk (the MCD model), the relation $L_{X,MCD} \propto T_{in}^4$ is obtained, which is interpreted that the innermost disk radius remains constant against varying accretion rates in the state (Shakura, & Sunyaev 1973; Ebisawa et al. 1993; Gierliński, & Done 2004). If a system has a slim disk (the Kawaguchi model), the relation $L_{X,MCD} \propto T_{in}^{\beta}$ is obtained, where $\beta \lesssim 4$ (Watarai et al. 2000). The power β decreases from 4 as an increasing mass accretion rate (Watarai et al. 2001). For samples with a successful fit by the MCD or Kawaguchi model or both, we derived the best-fit M_{BH} value and examined if it is consistent among all samples belonging to a source.

5.2.1. NGC 4490/85 ULX-8

We consider that ULX-8 exhibited an intra-state variation within the *bright* state. This is because the luminosity variation ($4.6\text{--}6.0 \times 10^{39}$ ergs s^{-1}) happens only above the border luminosity.

We speculate that this ULX is in the slim disk state based on the two lines of evidence. The first is that the scatter in the $L_{X,MCD}\text{--}T_{in}$ plot (Figure 6e) follows $L_{X,MCD} \propto T_{in}^{\beta}$, where $\beta = 1.0^{+0.7}_{-0.4}$. The value is consistent with the slim disk ($\beta \lesssim 4$) and not with the standard disk ($\beta \sim 4$). We note that the value is not an apparent slope caused by an additional spectral component (e.g. an additional PL component generally found in the HSS), because we obtained an even flatter slope ($\beta = 0.6^{+0.7}_{-0.3}$) when the spectra were fitted by two component models (the PL plus the MCD). Here, we fixed the photon index of the additional PL component to be 2.0 for the lack of statistics to constrain the value.

The second evidence is that a BH mass consistent among all the samples is found for the Kawaguchi model, but not for the MCD model. Figure 7 shows the best-fit parameters using the MCD and Kawaguchi models. In the MCD fitting (Figure 7a), a value $(R_{in}/\text{km})^2/(D/10 \text{ kpc})^2 (\cos i)^{-1} \propto M_{BH}^2$ consistent among the four samples was not found within 90% statistical uncertainty, which is unphysical. In other words, although spectra of ULXs in the *bright* state are commonly analyzed using the MCD model (e.g. Kubota et al. 2001), it now turns out that the MCD model does not describe the long-term spectral variations of the *bright* state. On the other hand, in the Kawaguchi model fitting (Figure 7b), the range $M_{BH} = 35\text{--}38 M_{\odot}$ was found

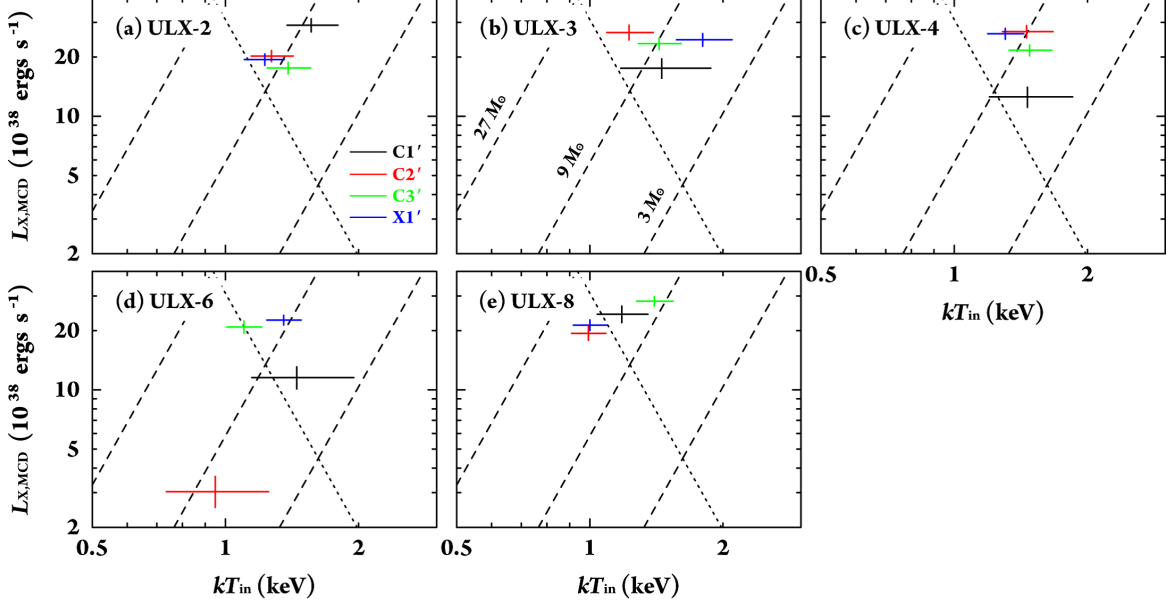


FIG. 6.— Plot of X-ray luminosity $L_{X,MCD}$ against the innermost disk temperature kT_{in} based on the MCD fitting results. The results of different observations are shown in different colors. The dashed lines show the $L_{X,MCD} \propto T_{in}^4$ relation with several representative masses, while the dotted line indicates the Eddington luminosity for the standard disk.

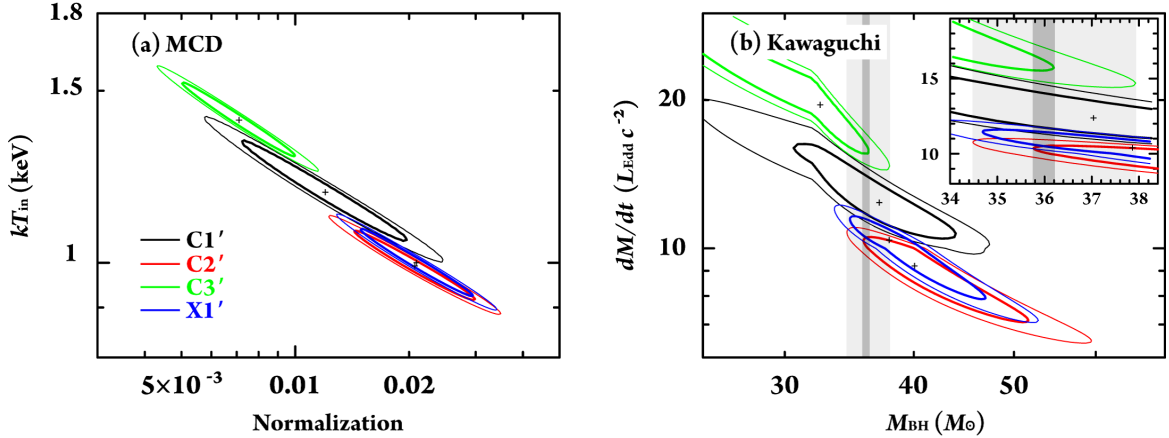


FIG. 7.— Significance contours of the best-fit physical parameters by two different models for NGC 4490/85 ULX-8; (a) kT_{in} versus the normalization ($\propto M_{BH}^2$) by the MCD model. (b) dM/dt versus M_{BH} by the Kawaguchi model. The results in different observations are shown with different colors: C1' (black), C2' (red), C3' (green), and X1' (blue). The two confidence levels are shown for 68% (thick solid) and 90% (thin solid) ranges for the two parameters. The inset at the top right in (b) is a close-up view of the center in the linear scale. The dark and light gray shaded ranges indicate the common M_{BH} ranges among the four samples with a 68% and 90% confidence, respectively.

to be consistent within 90% among the four samples. Thus, at least for this source, the Kawaguchi model is a more favorable description for its spectral variation.

Now we found a common BH mass range acceptable for the four samples, we fitted the four spectra by tying the BH mass to obtain a more stringent constraint. The best-fit value of M_{BH} is $37 \pm 2 M_{\odot}$ (Table 6). Resultantly, the Eddington ratio (L_X/L_{Edd}) is 0.41–0.63, which is similar to those of other ULX spectra considered to be in the slim disk state (0.36 for NGC 1313 X-2 and 0.52 for NGC 4559 X-7; Vierdayanti et al. 2006).

5.2.2. M51 Source-82

Source-82 shows variability among samples, which we consider to be an intra-state origin within the *faint* state. This is because the luminosity variation (1.6 – 2.9×10^{39} ergs s^{-1}) happens only below the border lu-

TABLE 6
BEST-FIT PARAMETERS OF THE KAWAGUCHI MODEL
FOR ULX-8.

Data label	N'_H (10^{22} cm $^{-2}$)	dM/dt (L_{Edd} c $^{-2}$)	$L_{X,Kaw}$ (10^{38} ergs s^{-1})
C1'	$0.68^{+0.10}_{-0.09}$	12^{+2}_{-1}	30 ± 3
C2'	$0.55^{+0.07}_{-0.06}$	10^{+1}_{-1}	22^{+3}_{-2}
C3'	$0.68^{+0.06}_{-0.06}$	15^{+2}_{-1}	36 ± 2
X1'	$0.38^{+0.05}_{-0.04}$	11^{+1}_{-1}	26^{+3}_{-2}
M_{BH}^a (M_{\odot})			37 ± 2
Red- χ^2 (d.o.f.)			1.04(143)

^a The BH mass is fixed among the four independent fittings.

minosity.

We consider that the source stayed in the state represented by the PL model in all samples based on the

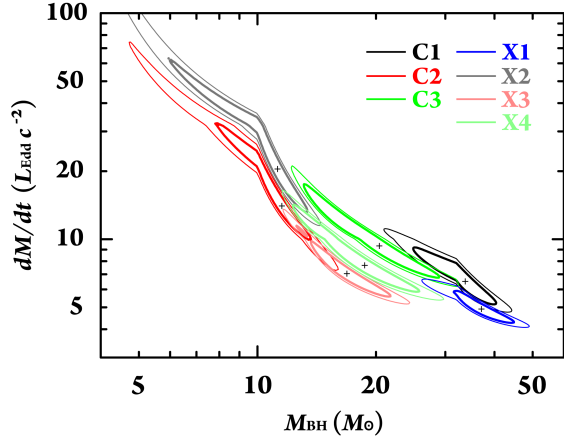


FIG. 8.— Significance contours of the best-fit physical parameters (dM/dt versus M_{BH}) by the Kawaguchi model for M51 source-82; The results in different observations are shown with different colors: C1 (black), C2 (red), C3 (green), X1 (blue), X2 (gray), X3 (light red), and X4 (light green). The two confidence levels are shown for 68% (thick solid) and 90% (thin solid) ranges.

following three reasons: (i) The majority of samples (six out of all seven) are successfully explained by a PL model. (ii) None of the samples is explained by an MCD model. (iii) Although the Kawaguchi model reproduces all the samples, the model is unlikely because we do not find M_{BH} consistent among all the samples (Figure 8).

In one sample (X1), source-82 shows a steep photon index of $2.6^{+0.3}_{-0.2}$ (Table 4). In contrast, in the other six samples, the derived index ($\Gamma \sim 1.8$ – 2.2 ; Table 4) is flatter than that in X1.

5.2.3. M51 Source-69

Source-69 clearly caused an inter-state transition. This ULX exhibits the largest luminosity variation by at least a factor of 70, and shows a transition among the *bright* state (X2, X3, and X4; 4.0 – 5.8×10^{39} ergs s^{-1}), the *faint* state (C1 and C3; 2.6 – 2.9×10^{39} ergs s^{-1}), and the *dim* state (C2 and X1; $< 1.2 \times 10^{39}$ ergs s^{-1}).

We discuss the representative model for the three states of the ULX. First, in the *bright* state, none of the PL, MCD, and Kawaguchi models explains all the three samples (Table 4). In particular, two samples (X3 and X4) were not reproduced by any models. We employed two component models (the PL plus the MCD or the Kawaguchi model), which did not improve the fit. The representative model was not found for this source in this state.

Second, the PL is the representative model for the *faint* state, because it is the only model to reproduce spectra of all samples. The derived index is quite flat of $\Gamma < 1.5$.

Finally, for the *dim* state, any models can reproduce the spectra and the representative model was not constrained. We note, however, that the spectra in this state is softer ($\Gamma \sim 1.9$ – 3.1) than in the other two states ($\Gamma < 1.7$).

5.2.4. NGC 4490/85 ULX-6

We consider that ULX-6 caused an inter-state transition because the variation spans the three different luminosity ranges as M51 source-69: the *bright* state (C3' and X1'; 4.4 – 5.3×10^{39} ergs s^{-1}), the *faint* state (C1'; $\sim 2.3 \times 10^{39}$ ergs s^{-1}), and the *dim* state (C2'; $\sim 7.2 \times 10^{38}$ ergs s^{-1}).

For the *bright* state, both the MCD and the Kawaguchi models can explain all the spectra, and yielded a BH mass consistent among the two samples. However, the flat slope ($\beta = 0.4^{+1.7}_{-0.6}$) of the $L_{\text{X,MCD}}-T_{\text{in}}$ plot (Figure 6d) favors the slim disk interpretation ($\beta \lesssim 4$). Thus, the representative model of the ULX in this state is expected to be the Kawaguchi model. We tried a simultaneous fitting by tying the M_{BH} value using the Kawaguchi model, and obtained the best-fit BH mass of $33^{+2}_{-5} M_{\odot}$. The Eddington ratio is 0.53 – 0.55 .

For the *faint* and *dim* states, all the models can explain all the samples, thus the representative model was not constrained. In the *dim* state, the PL fitting yielded the best-fit power of ~ 2.6 , which is similar to that found in the *dim* state of M51 source-69.

5.2.5. NGC 4490/85 the other ULXs

The remaining three sources have no clear features, thus the representative model and the BH mass can hardly be constrained. We briefly describe these sources.

Both ULX-2 and ULX-3 show intra-state variation as their luminosity ($L_{\text{X,PL}} \sim 3.3$ – 5.2 and 3.5 – 5.8×10^{39} ergs s^{-1} , respectively) stays in the *bright* state. For ULX-2, no model explains all the samples, thus the representative model was not found for this source. For ULX-3, any models can reproduce all the spectra. The $L_{\text{X,MCD}}-T_{\text{in}}$ plot does not separate the slim disk or the standard disk state, because the data cannot be fitted with a linear relation. A BH mass consistent among all the samples is found both for the MCD and the Kawaguchi models as $8 \pm 1 M_{\odot}$ and $28^{+6}_{-7} M_{\odot}$, respectively.

ULX-4, on the other hand, is considered to have exhibited an inter-state transition. The luminosities of the three samples are in the *bright* state (C2', C3', and X1'; 4.2 – 5.1×10^{39} ergs s^{-1}), while that of the other is in the *faint* state (C1'; $\sim 2.5 \times 10^{39}$ ergs s^{-1}). In both states, any models explain most of the samples, and the representative model cannot be constrained for the same reasons as ULX-3. If we estimate the BH mass using a simultaneous fitting of the two samples in the *bright* state, the BH mass is obtained as $9 \pm 1 M_{\odot}$ (MCD) and $26^{+6}_{-10} M_{\odot}$ (Kawaguchi).

5.3. Relations with Galactic BHBs

Many previous studies (e.g. Kubota et al. 2001; Dewangan et al. 2005; Winter et al. 2006; Vierdayanti et al. 2006; Gladstone, & Roberts 2009; Godet et al. 2009) suggested that the states of ULXs are related to those of Galactic BHBs. In the present study, we uniformly analyzed 34 spectra of seven ULXs in two interacting galaxies. As shown in § 5.2, we found some patterns of luminosity and spectral variations. We proceed to compare each state of the ULXs with those of Galactic BHBs.

For the *bright* state, especially for NGC 4490/85 ULX-8 and 6, we speculate that this state corresponds to the ASS based on the following two reasons: (i) The two sources with the slim disk are the most likely interpretation (§ 5.2.1 and 5.2.4). (ii) The Eddington ratios (0.41 – 0.63 and 0.53 – 0.55) are similar to those of two Galactic BHBs considered to be in the ASS: XTE J1550–564 (~ 0.4 ; Kubota, & Makishima 2004) and 4U 1630–47

(0.25–0.35; Abe et al. 2005). However, the *bright* state of M51 source-69 and NGC 4490/85 ULX-2 do not show such features of the ASS. This fact suggests that the boundary luminosity to separate the bright and the faint states may be correct overall, but varies source to source.

For the *faint* state, the representative model is PL for sources which we can determine a model (M51 source-82 and 69). The VHS and the LHS in Galactic BHBs have a PL shaped spectrum with the photon index Γ of ~ 2.5 and 1.5 – 1.9 , respectively. However, our samples in the *faint* state show a wide PL index range of $\Gamma \sim 1.1$ – 2.6 . Because a state with such a steep index of 1.1 has not been known so far, the *faint* state may be different from the well-known state in Galactic BHBs.

Finally, we briefly mention the *dim* state. We consider the *dim* state seen in some sources is distinctive from the *faint* states. This is because this state has lower luminosity and steeper spectral index, when fitted with PL, than the faint state. The photon statistics is too low to constrain the representative model, and their counterpart state in the Galactic BHBs is unknown.

6. SUMMARY AND CONCLUSIONS

We have analyzed X-ray spectra (34 samples) of seven bright ULXs in the interacting galaxy systems M51 and NGC 4490/85 using the archived data from multiple *Chandra* and *XMM-Newton* observations. We constructed a histogram of luminosities, in which we found a hint of three distinctive states: (i) The *bright* state with the brighter luminosity range (3 – 6×10^{39} ergs s $^{-1}$) for 20 samples, (ii) the *faint* state with the fainter luminosity range (1.5 – 3×10^{39} ergs s $^{-1}$) for 11 samples, and (iii) the *dim* state with luminosities below the fainter range ($< 1.2 \times 10^{39}$ ergs s $^{-1}$) for three samples. On the whole, the spectra in the *bright* state are represented by the MCD model (standard disk) or the Kawaguchi model (slim disk), while those in the *faint* state are represented by the PL model. We classified the flux changes of all sources into the intra-state variation and the inter-state transition. Four ULXs (M51 source-82, NGC 4490/85 ULX-2, 3, and 8) exhibited the former, while the remaining three (M51 source-69, NGC 4490/85 ULX-4, and 6)

exhibited the latter.

All the spectra of two ULXs (NGC 4490/85 ULX-8 and 6) in the *bright* state can be reproduced by a slim disk model by Kawaguchi (2003) with a constant BH mass of 37 ± 2 and $33_{-5}^{+2} M_{\odot}$, respectively. In particular, for ULX-8, a common BH mass was not found with the MCD model fitting. This suggests that the slim disk model is a more appropriate explanation at least in some cases of the “*bright*” state, in which ULXs harbor BHs of a mass of $< 40 M_{\odot}$.

From the results of spectral fitting, we compare each state of the ULXs with those of Galactic BHBs. We propose that the *bright* state of two ULXs (NGC 4490/85 ULX-8 and 6) corresponds to the ASS of Galactic BHBs. For the *faint* state, the representative model is PL. However, it is different in the range of photon index from the VHS of Galactic BHBs, which also shows a PL spectrum. We thus consider that the *faint* state is unique to ULXs. The nature of the *dim* state is unconstrained, but has the most steep spectrum.

We thank the anonymous reviewer for critical comments for the paper. This research has made use of public data and software obtained from the High Energy Astrophysics Science Archive Research Center (HEASARC), provided by NASA’s Goddard Space Flight Center. Funding for the SDSS and SDSS-II has been provided by the Alfred P. Sloan Foundation, the Participating Institutions, the National Science Foundation, the U.S. Department of Energy, the National Aeronautics and Space Administration, the Ministry of Education, Culture, Sports, Science, and Technology of Japan, the Max Planck Society, and the Higher Education Funding Council for England. The SDSS Web Site is <http://www.sdss.org/>. SDSS images used in this paper was produced with Montage, an image mosaic service supported by the NASA Earth Sciences Technology Office Computing Technologies program. Tessei Yoshida is supported by the Japan Society for the Promotion of Science Research Fellowship for Young Scientists.

Facilities: CXO (ACIS), XMM (EPIC).

REFERENCES

- Abe, Y., Fukazawa, Y., Kubota, A., Kasama, D., & Makishima, K. 2005, PASJ, 57, 629
- Abramowicz, M. A., Czerny, B., Lasota, J. P., & Szuszkiewicz, E. 1988, ApJ, 332, 646
- Brassington, N. J., Ponman, T. J., & Read, A. M. 2007, MNRAS, 377, 1439
- Broos, P. S., Townsley, L. K., Getman, K., & Bauer, F. E. 2002, ACIS Extract, An ACIS Point Source Extraction Package (University Park: Pennsylvania State Univ.)
- Clemens, M. S., Alexander, P., & Green, D. A. 1998, MNRAS, 297, 1015
- Clemens, M. S., Alexander, P., & Green, D. A. 1999, MNRAS, 307, 481
- Clemens, M. S., & Alexander, P. 2002, MNRAS, 333, 39
- Davis, S. W., Done, C., & Blaes, O. M. 2006, ApJ, 647, 525
- Dewangan, G. C., Griffiths, R. E., Choudhury, M., Miyaji, T., & Church, N. J. 2005, ApJ, 635, 198
- Dickey, J. M., & Lockman, F. J. 1990, ARA&A, 28, 215
- de Vaucouleurs, G., de Vaucouleurs, A., & Corwin, J. R. 1976, Second Reference Catalogue of Bright Galaxies (Austin: Univ. Texas Press)
- de Vaucouleurs, G., de Vaucouleurs, A., Corwin, H. G., Jr., Buta, R. J., Paturel, G., & Fouque, P. 1991, Third Reference Catalogue of Bright Galaxies (New York: Springer)
- Ebisawa, K., Makino, F., Mitsuda, K., Belloni, T., Cowley, A. P., Schmidtke, P. C., & Treves, A. 1993, ApJ, 403, 684
- Ebisawa, K., et al. 1994, PASJ, 46, 375
- Ebisawa, K., Życki, P., Kubota, A., Mizuno, T., & Watarai, K. 2003, ApJ, 597, 780
- Ehle, M., Pietsch, W., & Beck, R. 1995, A&A, 295, 289
- Esin, A. A., McClintock, J. E., & Narayan, R. 1997, ApJ, 489, 865
- Fabbiano, G. 2006, ARA&A, 44, 323
- Feldmeier, J. J., Ciardullo, R., & Jacoby, G. H. 1997, ApJ, 479, 231
- Feng, H., & Kaaret, P. 2010, ApJ, 712, L169
- Foschini, L., et al. 2006, Advances in Space Research, 38, 1378
- Fridriksson, J. K., Homan, J., Lewin, W. H. G., Kong, A. K. H., & Pooley, D. 2008, ApJS, 177, 465
- Fukazawa, Y., Iyomoto, N., Kubota, A., Matsumoto, Y., & Makishima, K. 2001, A&A, 374, 73
- Garmire, G. P., Bautz, M. W., Ford, P. G., Nousek, J. A., & Ricker, G. R., Jr. 2003, Proc. SPIE, 4851, 28
- Gierliński, M., & Done, C. 2004, MNRAS, 347, 885
- Gladstone, J. C., & Roberts, T. P. 2009, MNRAS, 397, 124
- Goad, M. R., Roberts, T. P., Reeves, J. N., & Uttley, P. 2006, MNRAS, 365, 191
- Godet, O., Barret, D., Webb, N. A., Farrell, S. A., & Gehrels, N. 2009, ApJ, 705, L109

- Jansen, F., et al. 2001, *A&A*, 365, L1
- Kaaret, P., Prestwich, A. H., Zezas, A., Murray, S. S., Kim, D.-W., Kilgard, R. E., Schlegel, E. M., & Ward, M. J. 2001, *MNRAS*, 321, L29
- Kaaret, P., Ward, M. J., & Zezas, A. 2004, *MNRAS*, 351, L83
- Kawaguchi, T. 2003, *ApJ*, 593, 69
- King, A. R., Davies, M. B., Ward, M. J., Fabbiano, G., & Elvis, M. 2001, *ApJ*, 552, L109
- Kubota, A., Tanaka, Y., Makishima, K., Ueda, Y., Dotani, T., Inoue, H., & Yamaoka, K. 1998, *PASJ*, 50, 667
- Kubota, A., Mizuno, T., Makishima, K., Fukazawa, Y., Kotoku, J., Ohnishi, T., & Tashiro, M. 2001, *ApJ*, 547, L119
- Kubota, A., & Makishima, K. 2004, *ApJ*, 601, 428
- Kuno, N., & Nakai, N. 1997, *PASJ*, 49, 279
- Liu, J.-F., Bregman, J. N., Irwin, J., & Seitzer, P. 2002, *ApJ*, 581, L93
- Liu, J.-F., & Bregman, J. N. 2005, *ApJS*, 157, 59
- Maccarone, T. J. 2003, *A&A*, 409, 697
- Makishima, K., et al. 2000, *ApJ*, 535, 632
- Marston, A. P., Elmegreen, D., Elmegreen, B., Forman, W., Jones, C., & Flanagan, K. 1995, *ApJ*, 438, 663
- Matsumoto, H., Tsuru, T. G., Koyama, K., Awaki, H., Canizares, C. R., Kawai, N., Matsushita, S., & Kawabe, R. 2001, *ApJ*, 547, L25
- McClintock, J. E., Narayan, R., & Shafee, R. 2007, *Black Holes* (Cambridge: Cambridge Univ. Press), arXiv:0707.4492
- Miller, M. C., & Colbert, E. J. M. 2004, *International Journal of Modern Physics D*, 13, 1
- Mitsuda, K., et al. 1984, *PASJ*, 36, 741
- Miyawaki, R., Makishima, K., Yamada, S., Gandhi, P., Mizuno, T., Kubota, A., Tsuru, T. G., & Matsumoto, H. 2009, *PASJ*, 61, 263
- Mizuno, T., et al. 2007, *PASJ*, 59, 257
- Morrison, R., & McCammon, D. 1983, *ApJ*, 270, 119
- Ohsuga, K., Mori, M., Nakamoto, T., & Mineshige, S. 2005, *ApJ*, 628, 368
- Okajima, T., Ebisawa, K., & Kawaguchi, T. 2006, *ApJ*, 652, L105
- Palumbo, G. G. C., Fabbiano, G., Trinchieri, G., & Fransson, C. 1985, *ApJ*, 298, 259
- Pringle, J. E. 1981, *ARA&A*, 19, 137
- Ptak, A., Serlemitsos, P., Yaqoob, T., & Mushotzky, R. 1999, *ApJS*, 120, 179
- Ptak, A., & Griffiths, R. 1999, *ApJ*, 517, L85
- Read, A. M., Ponman, T. J., & Strickland, D. K. 1997, *MNRAS*, 286, 626
- Roberts, T. P., & Warwick, R. S. 2000, *MNRAS*, 315, 98
- Roberts, T. P., Warwick, R. S., Ward, M. J., & Murray, S. S. 2002, *MNRAS*, 337, 677
- Roberts, T. P., Kilgard, R. E., Warwick, R. S., Goad, M. R., & Ward, M. J. 2006, *MNRAS*, 371, 1877
- Schweizer, F. 1977, *ApJ*, 211, 324
- Scoville, N. Z., Polletta, M., Ewald, S., Stolovy, S. R., Thompson, R., & Rieke, M. 2001, *AJ*, 122, 3017
- Shakura, N. I., & Sunyaev, R. A. 1973, *A&A*, 24, 337
- Shimura, T., & Takahara, F. 1995, *ApJ*, 445, 780
- Strüder, L., et al. 2001, *A&A*, 365, L18
- Terashima, Y., Ptak, A., Fujimoto, R., Itoh, M., Kunieda, H., Makishima, K., & Serlemitsos, P. J. 1998, *ApJ*, 496, 210
- Terashima, Y., & Wilson, A. S. 2004, *ApJ*, 601, 735
- Terashima, Y., Inoue, H., & Wilson, A. S. 2006, *ApJ*, 645, 264
- Tsunoda, N., Kubota, A., Namiki, M., Sugiho, M., Kawabata, K., & Makishima, K. 2006, *PASJ*, 58, 1081
- Turner, M. J. L., et al. 2001, *A&A*, 365, L27
- van der Hulst, J. M., Kennicutt, R. C., Crane, P. C., & Rots, A. H. 1988, *A&A*, 195, 38
- Vázquez, G. A., Hornschemeier, A. E., Colbert, E., Roberts, T. P., Ward, M. J., & Malhotra, S. 2007, *ApJ*, 658, L21
- Viallefond, F., Allen, R. J., & de Boer, J. A. 1980, *A&A*, 82, 207
- Vierdayanti, K., Mineshige, S., Ebisawa, K., & Kawaguchi, T. 2006, *PASJ*, 58, 915
- Watarai, K., Fukue, J., Takeuchi, M., & Mineshige, S. 2000, *PASJ*, 52, 133
- Watarai, K., Mizuno, T., & Mineshige, S. 2001, *ApJ*, 549, L77
- Weisskopf, M. C., Brinkman, B., Canizares, C., Garmire, G., Murray, S., & Van Speybroeck, L. P. 2002, *PASP*, 114, 1
- Winter, L. M., Mushotzky, R. F., & Reynolds, C. S. 2006, *ApJ*, 649, 730